Publ. Astron. Soc. Japan 39, 57–68 (1987)

CO and H I Correlation in Superclouds of M 31*

Makoto NAKANO and Takashi ICHIKAWA

Department of Astronomy, Faculty of Science, University of Kyoto, Sakyo-ku, Kyoto 606

Yutaka D. TANAKA

Kobe Yamate Women's Junior College, Suwayama, Chuo-ku, Kobe 650

and

Naomasa NAKAI and Yoshiaki SOFUE

Nobeyama Radio Observatory, Minamimaki-mura, Minamisaku-gun, Nagano 384-13
and
Department of Astronomy, Faculty of Science, University of Tokyo, Bunkyo-ku, Tokyo 113

(Received 1986 March 12; accepted 1986 August 30)

Abstract

^{12}CO (J=1–0) observations with a resolution of 47 pc made with the Nobeyama 45-m telescope resolved a super CO cloud in a spiral arm of M31. The CO cloud associated with a super H I cloud extends over 1 kpc along the spiral arm. The width of CO arm is, however, less than 500 pc, much narrower than the H I arm width of 1–2 kpc. A strong correlation is found between the surface mass densities of H I and H_2 gases in the supercloud. The ratio of the surface density of H_2 to the total gas density of H I and H_2 increases from 0.4 to 0.7 with the total gas density. The result suggests that the excess of H I gas over about 10 $M_\odot$ pc^{-2} is converted to H_2 molecules. These facts give evidence of a transient phenomenon of gases the in the supercloud.

Key words: CO; Galaxies; H I; M31.

1. Introduction

Elmegreen and Elmegreen (1983) studied giant H II regions and H I clouds in galaxies to determine the dimension of clouds and star forming regions. They have noted that coherent star forming region has a size as large as a kiloparsec or more, and called this large and fundamental structure a *supercloud.* The small distance to M31, 690 kpc, is advantageous for the study of the internal structure of such superclouds. Many authors have studied optical appearances of spiral arms of M31 (cf.

* Based on observations made at the Nobeyama Radio Observatory (NRO). NRO, a branch of the Tokyo Astronomical Observatory, University of Tokyo, is a facility open for general use by researchers in the field of astronomy, astrophysics, and astrochemistry.

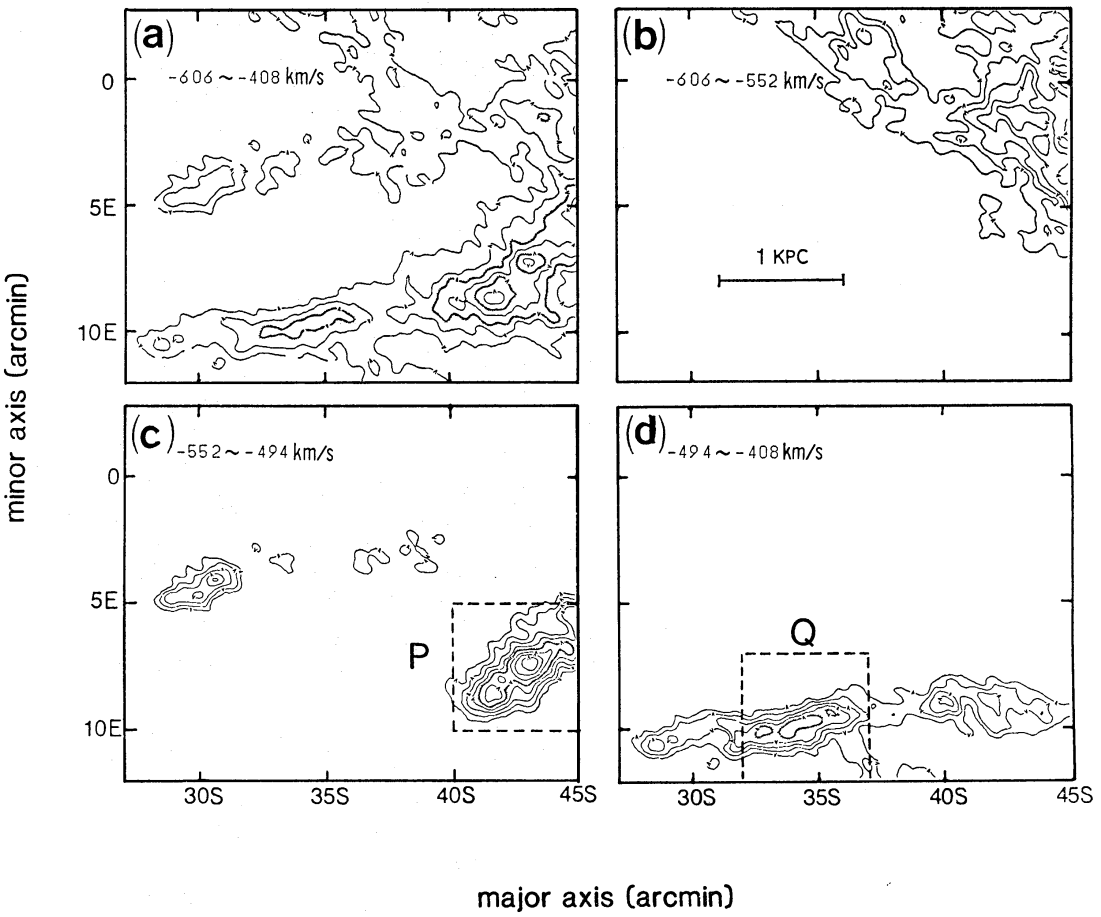

Fig. 1. Contour maps of integrated H I emission in each velocity range of the southern part of M31 reproduced from the H I data published by Brinks and Shane (1984). The spatial resolution is 24″×36″ (80 pc×120 pc). The lowest contour is 500 K km s^{-1} for (b) and 1000 K km s^{-1} for the others. The contour interval is 500 K km s^{-1} for (a) and 250 K km s^{-1} for the others. The boxes enclosed by the dashed lines indicate our investigated regions which are shown in figure 2.

Baade and Arp 1964; Pellet et al. 1978). Brinks (and Shane 1984) have made H I observations of M31 with a resolution of 24″×36″, 80 pc×120 pc, at the distance of M31. The integrated H I-line emission in the south of M31 shows several large cloud-like structures with sizes ranging from hundreds to a thousand parsecs tracing the spiral arms and dust lanes (P and Q in figure 1). The structures recall the super-cloud as noted by Elmegreen and Elmegreen (1983).

However, since molecular clouds play a crucial role in the star formation process, a 21-cm H I line study is not sufficient to know the nature of the star formation in the spiral arms. An extensive CO map of the southeastern part of M31 was obtained by Stark (1985). Ichikawa et al. (1987) have compiled data on H I and CO observations, visual extinction, OB associations, H II regions, and thermal infrared radiation from IRAS in the region. They showed that the superclouds form a region of coherent star formation. The CO distribution is similar to that of H I gas and forms cloudlike structures as large as the super H I clouds. Recently Boulanger et al. (1984) and Ichikawa et al. (1985, hereafter referred to as paper I) studied the CO emission in the

superclouds using large millimeter-wave telescopes with a high spatial resolution.

In this paper we present additional ^{12}CO ($J=1$–0) observations in the superclouds of M31 with a resolution of 14″. This resolution corresponds to a linear size of 47 pc at the distance of M31 and is small enough to resolve the spatial and velocity distributions of the CO clouds. Using the H I data of Brinks and Shane (1984), we investigate the correlation of the distribution and surface densities of neutral and molecular hydrogen gases.

2. CO Observations

The additional observations of $J=1$–0 line of ^{12}CO were made in 1985 February using the 45-m millimeter-wave telescope at the Nobeyama Radio Observatory (NRO). The half-power beam width of the telescope was 14″ at this frequency. A He-cooled receiver with a Schottky barrier diode mixer with a single side band was employed and provided a system temperature of $T=600$ K. Data was collected by an acousto-optical spectrometer with 2048 channels of 250-kHz resolution. This corresponds to a velocity resolution of 0.65 km s^{-1} at 115 GHz. The efficiency of the main beam and the aperture of the antenna at 115 GHz was about 0.3 and 0.25, respectively. The telescope was operated in a position-switch mode. The calibration of the data was accomplished by referring to an ambient temperature absorber in front of the receiver. Each point was observed for about one hour. We checked the temperature scale by observing at the reference position, P13, of paper I and Orion A. The pointing accuracy was checked every two hours by measuring the 43-GHz SiO maser line of

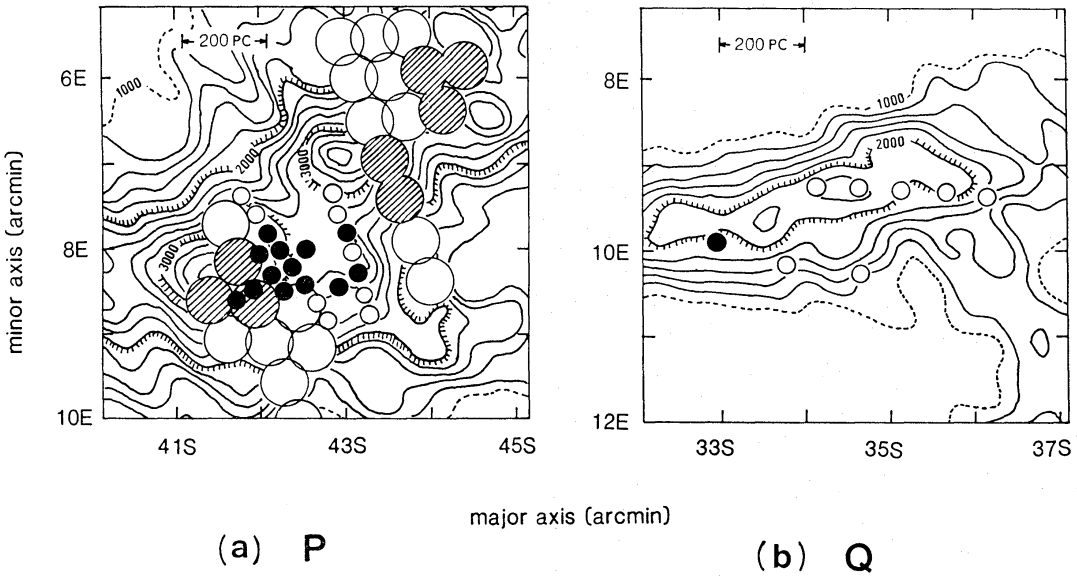

Fig. 2. Positions of CO observations in super H I clouds (a) P and (b) Q, superposed on the contour map of the H I emission integrated between −604 km s^{-1} and −356 km s^{-1}. The unit of the contour level is in K km s^{-1}. The size of the circles shows the beam size. The small and large circles correspond to our observations (paper I and the present paper) with a 47-pc resolution by the 45-m telescope and those of Boulanger et al. (1984) with a 100-pc resolution by the Onsala 20-m telescope, respectively. Filled and hatched circles represent the region where CO emission was detected.

EY And and confirmed to be within 10″. We observed 8 points in P and 8 points in Q. The newly observed points and those of paper I are shown in figure 2 with circles. The circles of 14″ and 33″ in diameter superposed on the integrated H I intensity contours of Brinks and Shane (1984) represent the spatial resolution of our observations and that of Boulanger et al. (1984), respectively. Filled and hatched circles designate the points where the CO emission was detected. X and Y are the directions of the major and minor axes of M31 following the coordinates of Brinks and Shane (1984).

3. Results

The newly observed CO emissions are displayed in figure 3, where the velocity resolution is reduced to 1.3 km s^{-1}. The velocity is given by heliocentric value. The observational results are summarized in table 1.

Table 1. Observational results.

Observed point	Position† ($\Delta\alpha$, $\Delta\delta$)	T_A* (K)	σ_{rms} (K)	V_{peak} (km s^{-1})
P15	(−49″, 166″)	...	0.13	...
P16	(−40 , 154)	...	0.09	...
P17	(−31 , 142)	0.34	0.10	−515
P18	(−22 , 130)	...	0.13	...
P19	(−13 , 118)	0.39	0.12	−520
P20	(− 4 , 106)	...	0.12	...
P21	(5 , 94)	...	0.11	...
P22	(2 , 123)	0.46	0.12	−469
Q1	(17 , 25)	...	0.11	...
Q2	(0 , 0)	...	0.17	...
Q3	(−17 , −25)	...	0.17	...
Q4	(−34 , −50)	...	0.17	...
Q5	(−50 , −75)	...	0.11	...
Q6	(90 , 56)	0.42	0.10	−449
Q7	(75 , 9)	...	0.10	...
Q8	(45 , −38)	...	0.11	...

† Offset position from P4 ($\alpha_{1950}=0^h38^m17^s.1$, $\delta_{1950}=+40°21'39''$; paper I) for P and offset position from Q2 ($\alpha_{1950}=0^h38^m47^s.3$, $\delta_{1950}=+40°26'38''$) for Q.

Table 2. Quantities for the observed emission features.

Observed point	Velocity range (V_1, V_2) (km s^{-1})	$\langle V\rangle_{CO}$ (km s^{-1})	ΔV (km s^{-1})	$\langle V\rangle_{CO}-V_{rot}$ (km s^{-1})	$\int_{V_1}^{V_2} T_A^* dV$ (K km s^{-1})	N_{H_2} (10^{20} cm^{-2})	σ_{H_2} ($M_\odot$ pc^{-2})
P17	(−533, −488)	−512	17	−11	13.2	10.7	17
P19a	(−527, −514)	−521	5	−16	4.7	3.8	6
P19b	(−513, −504)	−508	4	−12	3.1	2.5	4
P22	(−475, −467)	−471	2	−22	4.3	3.5	6
Q6	(−466, −429)	−447	11	+ 8	7.9	6.4	10
	(−452, −440)	−446	5	+ 8	5.1	4.1	7

Table 3. Quantities for the H I emission.

Observed point	Position* (X, Y)	Velocity range (V_1, V_2) (km s^{-1})	$\langle V\rangle_{HI}$ (km s^{-1})	ΔV (km s^{-1})	$\langle V\rangle_{HI}-V_{rot}$ (km s^{-1})	$\int_{V_1}^{V_2} T_b dV$ (K km s^{-1})	N_{HI} (10^{20} cm^{-2})	σ_{HI} ($M_\odot$ pc^{-2})
P 1	(42.5E, 8.0S)	(−556, −499)	−523	21	−27	1698	7.0	5.7
		(−499, −449)	−482	17	14	1150	4.7	3.9
P 2	(41.8 , 7.3)	(−569, −478)	−515	33	−12	2401	9.9	8.1
P 3	(42.0 , 7.5)	(−560, −482)	−515	29	−14	2532	10.4	8.5
P 4	(42.1 , 7.8)	(−556, −461)	−511	29	−12	2738	11.2	9.2
P 5	(42.2 , 8.0)	(−552, −499)	−523	17	−27	1657	6.8	5.6
		(−499, −461)	−486	17	10	1102	4.5	3.7
P 6	(42.4 , 8.2)	(−552, −499)	−523	21	−29	1584	6.5	5.3
		(−499, −461)	−482	17	12	1163	4.8	3.9
P 7	(42.5 , 8.4)	(−552, −499)	−523	21	−31	1514	6.2	5.1
		(−499, −461)	−482	17	10	1128	4.6	3.8
P 8	(42.7 , 8.6)	(−544, −499)	−519	17	−29	1128	4.6	3.8
		(−499, −433)	−474	25	16	1458	6.0	4.9
P 9	(42.8 , 8.8)	(−544, −499)	−519	17	−32	992	4.0	3.3
		(−499, −433)	−474	25	13	1524	6.3	5.1
P10	(42.0 , 8.1)	(−556, −499)	−519	21	−24	1780	7.3	6.0
		(−499, −449)	−482	21	13	1320	5.4	4.5
P11	(42.1 , 8.3)	(−556, −503)	−523	25	−30	1601	6.6	5.4
		(−503, −457)	−486	21	7	1473	6.0	5.0
P12	(42.3 , 8.5)	(−556, −499)	−523	21	−32	1367	5.6	4.6
		(−499, −457)	−482	21	9	1187	4.9	4.0
P13	(41.9 , 8.4)	(−540, −457)	−503	41	−11	2776	11.4	9.4
P14	(41.7 , 8.6)	(−536, −457)	−499	37	− 9	2704	11.1	9.1
P15	(42.9 , 7.3)	(−556, −490)	−523	29	−16	2729	11.2	9.2

Table 3. (Continued)

Observed point	Position* (X, Y)	Velocity range (V_1, V_2) (km s^{-1})	$\langle V\rangle_{\rm HI}$ (km s^{-1})	ΔV (km s^{-1})	$\langle V\rangle_{\rm HI}-V_{\rm rot}$ (km s^{-1})	$\int_{V_1}^{V_2} T_b dV$ (K km s^{-1})	$N_{\rm HI}$ (10^{20} cm^{-2})	$\sigma_{\rm HI}$ ($M_\odot$ pc^{-2})
P16	(43.0E, 7.6S)	(−548, −478)	−519	33	−15	2267	9.3	7.6
P17	(43.0 , 7.8)	(−552, −503)	−523	21	−22	1612	6.6	5.4
P18	(43.1 , 8.0)	(−548, −494)	−523	21	−25	1652	6.8	5.6
		(−494, −433)	−470	33	28	1020	4.2	3.4
P19	(43.2 , 8.3)	(−548, −494)	−519	17	−24	1430	5.9	4.8
		(−494, −437)	−474	25	21	1168	4.8	3.9
P20	(43.2 , 8.5)	(−548, −494)	−519	21	−27	1066	4.4	3.6
		(−494, −437)	−474	25	18	1293	5.3	4.4
P21	(43.3 , 8.8)	(−540, −494)	−515	21	−25	751	3.1	2.5
		(−494, −428)	−470	29	20	1410	5.8	4.8
P22	(42.9 , 8.4)	(−548, −494)	−519	21	−26	1421	5.8	4.8
		(−494, −437)	−478	33	15	1156	4.6	3.8
Q1	(34.1 , 9.2)	(−503, −433)	−461	29	5	2135	8.8	7.2
Q2	(34.6 , 9.3)	(−490, −433)	−461	25	6	1975	8.1	6.7
Q3	(35.1 , 9.3)	(−503, −428)	−466	33	2	1885	7.7	6.4
Q4	(35.6 , 9.3)	(−507, −428)	−470	37	− 2	1810	7.4	6.1
Q5	(36.1 , 9.4)	(−523, −424)	−478	45	− 9	1561	6.4	5.3
Q6	(33.0 , 9.9)	(−499, −424)	−453	33	2	1909	7.8	6.4
Q7	(33.8 , 10.2)	(−507, −424)	−457	33	− 3	1454	6.0	4.9
Q8	(34.7 , 10.3)	(−470, −424)	−453	21	2	808	3.3	2.7

* Coordinates following Brinks and Shane (1984).

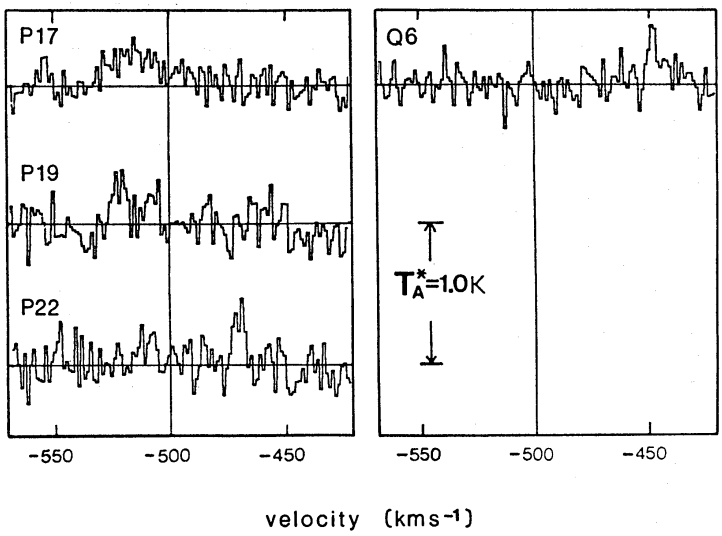

Fig. 3. Newly observed CO emissions for the points in superclouds P and Q listed in table 2. The velocity is given by heliocentric value. The velocity resolution is reduced to 1.3 km s^{-1}.

For the CO emission, we derived by the same procedure as in paper I the mean velocity $\langle V\rangle_{CO}$, the full velocity width at half intensity ΔV, the face-on column density of molecular hydrogen $N(H_2)$, and the face-on surface mass density $\sigma(H_2)$ in the range V_1 and V_2 presented in the second column from the integrated intensity of the observed CO emission. The results are presented in table 2. We also derived the same data for H I emission line from Brinks and Shane (1984) at the same positions as our CO observations (table 3). The face-on surface density of neutral hydrogen, σ (H I), was calculated from the integrated brightness temperature assuming that H I emission is optically thin.

4. Discussion and Conclusions

4.a. Size of a CO Cloud Complex in Superclouds

The largest super H I cloud P has an apparent size of 500 pc$\times$1 kpc (see figure 1). The mass of hydrogen is estimated to be $M(\text{H I})\approx 2\times 10^7\ M_\odot$ and $M(H_2)\approx 3\times 10^6\ M_\odot$ by Boulanger et al. (1981). From figure 2, a CO cloud complex in P is found to extend over 1 kpc as long as the H I cloud; this may be called a *super CO cloud.* The distribution of the surface densities of molecular and neutral hydrogen gases as a function of the galactocentric distance R across P is shown in figure 4. From this figure, we can confirm that the width of a super CO cloud is less than 500 pc, much narrower than the width 1–2 kpc of the H I cloud, although the H I width has been slightly smeared out due to the larger beam size. The CO observations with a resolution of 100 pc of Boulanger et al. (1984) have also supported this result. The narrow width suggests a transient phenomenon of gases in the supercloud.

We have observed 8 points in Q, which is less massive than P. The CO emission was detected only at the bright H II region, BA 297. No indication of CO emission was found at the place of the highest density of H I in Q, but this result is reasonable,

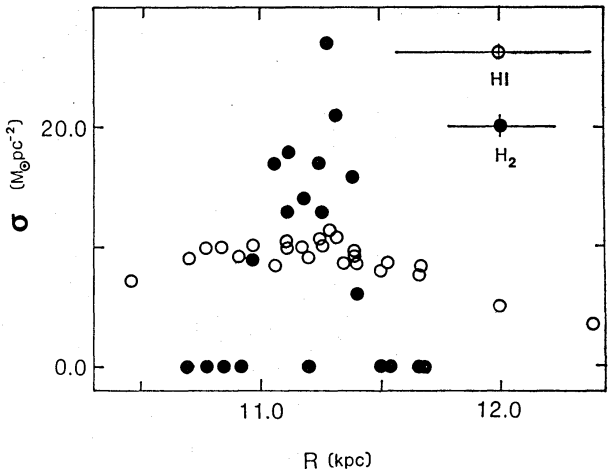

Fig. 4. Distributions of the face-on surface densities of H I (Brinks and Shane 1984) and H_2 (paper I and the present paper) across supercloud P as a function of the galactocentric distance R. The bars in the corner represent the spatial resolution in the R direction and the typical observational error in the integrated intensity.

because the H I density is much smaller than that of P. This result will be discussed in section 4c.

4.b. CO Emission in H II Regions

Our CO observations in paper I covered only a part of large and bright H II regions. In the present paper, we have observed CO at two bright and small H II regions, i.e., BA 313 (X=43.1S, Y=8.4E) and BA 297 (X=33.0S, Y=9.9E) (Baade and Arp 1964), which are associated with superclouds P and Q at the outer edges, re-

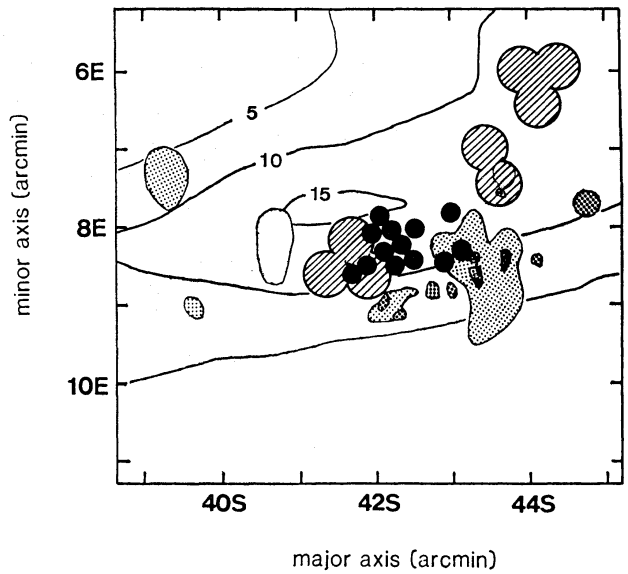

Fig. 5. Comparison of the CO emission region, H II regions (Pellet et al. 1978), and the contours of 25-μm emission obtained by IRAS (Habing et al. 1984) in supercloud P. The three grades of shading for the H II region follow the intensity levels of Pellet et al. (1978). The unit of 25-μm emission is 4.2×10^{-9} W m^{-2} sr^{-1}. The meaning of the symbols for CO emission is the same as in figure 2.

spectively. We have detected CO emissions on these H II regions (P22 and Q6). Blitz (1985) has surveyed the CO emission line in bright H II regions in M31. He also detected CO emission in BA 297 with $T_R^*=0.14$ K. Comparing with their result, we can show the existence of GMCs with a mass of $(1\text{–}5)\times10^4\ M_\odot$ in BA 297 of Q and in BA 313 of P. However, we can see in figure 5 that the strong CO emission regions avoid the H II region complexes. Contours of 25-μm emission observed by IRAS (Habing et al. 1984) are also shown in figure 5. The spiral armlike feature of 25-μm emission can be seen overlapped with the superclouds (figure 5). Although the spatial resolution of IRAS is too low—900 pc in the direction of the major axis and 150 pc in the direction of the minor axis at the distance of M31—to discuss the spatial difference between the CO and 25-μm emitting regions, the 2.5-μm emission suggests the existence of massive young stars embedded in the supercloud. To investigate the star forming activity in the molecular clouds, infrared observations with a much higher resolution should be made.

4.c. Correlation of CO and H I Line Emissions

H I emission at P has two velocity components at the mean radial velocities of -520 km s^{-1} and -480 km s^{-1} with the velocity difference reaching about 40 km s^{-1}. Figure 6 shows the contours of the H I emission intensity at $V=-519$ km s^{-1} and $V=-478$ km s^{-1}.

The distribution of two components is considerably different, as can be seen in figures 1 and 6. These two components are not due to the warp of H I disk (Brinks and Burton 1984). The central velocity of the warped disk at the position of P is about -450 km s^{-1} and the projected mass density of neutral hydrogen is negligible compared to that of the -480-km s^{-1} component. Figure 7 compares the H I profiles

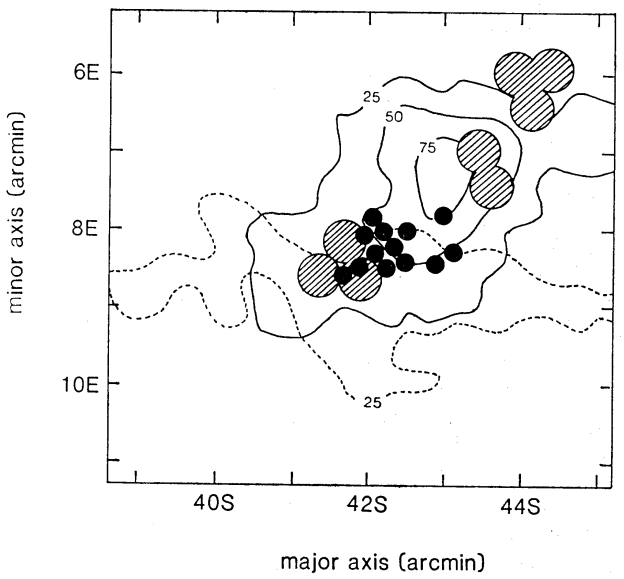

Fig. 6. Comparison of the CO emission region and two velocity components of H I emission in supercloud P. The contours are at -519 km s^{-1} (full lines) and -478 km s^{-1} (dashed lines) (Brinks and Shane 1984) in units of brightness temperature. The meaning of the symbols for CO emission is the same as in figure 2.

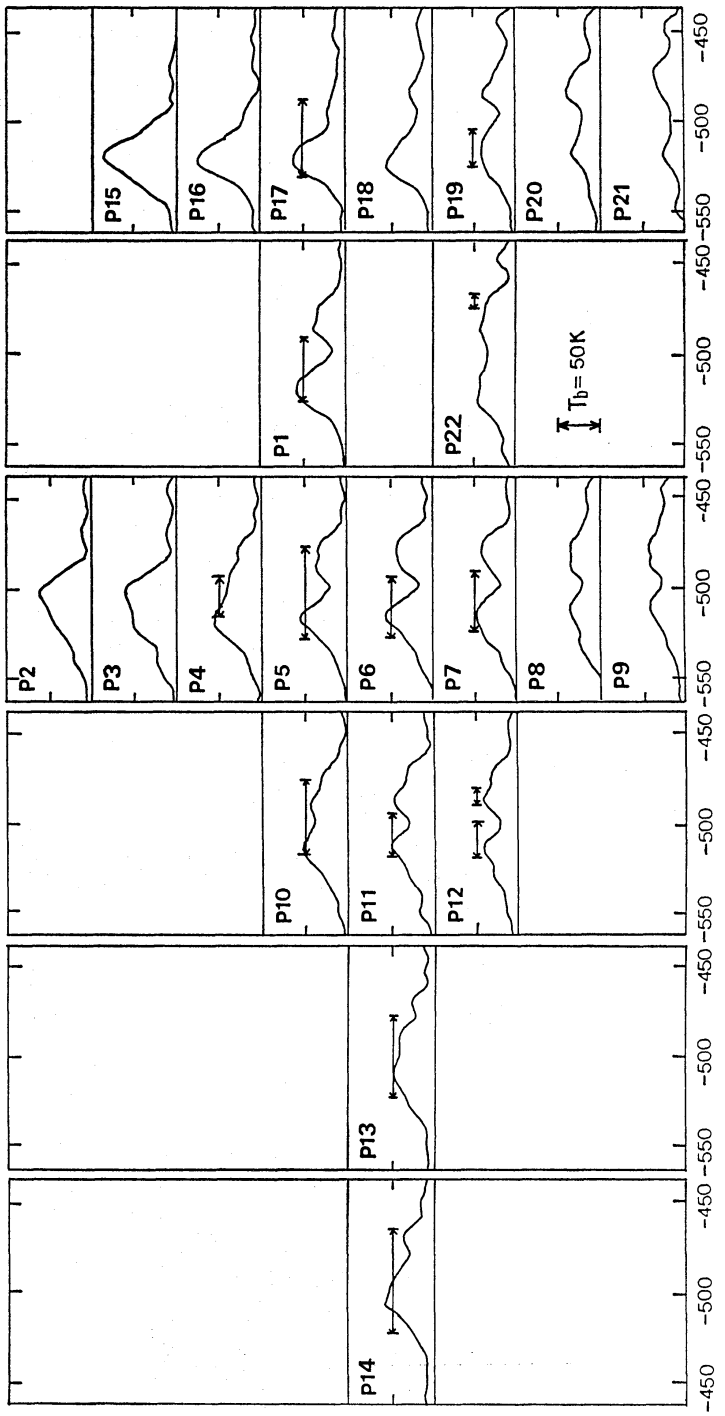

Fig. 7. H I line profiles of our observational points in supercloud P (Brinks and Shane 1984). The arrows indicate the full velocity range of the detected CO line emissions.

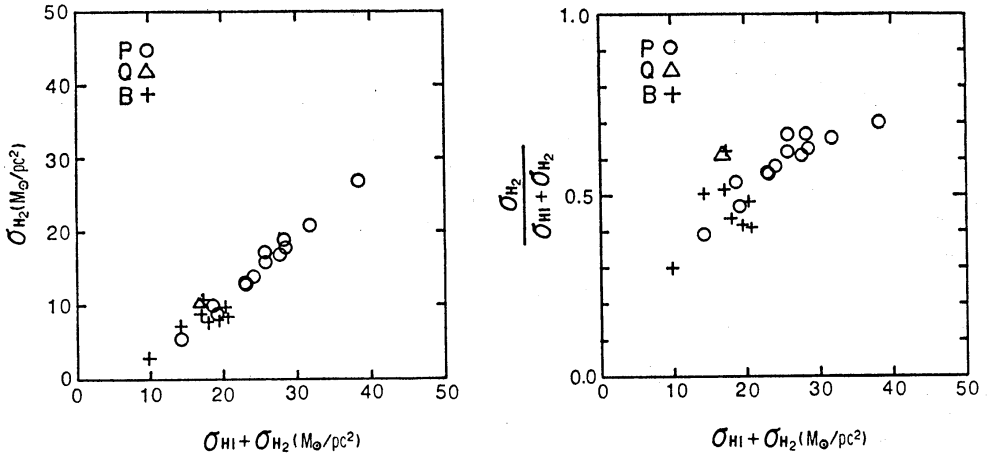

Fig. 8. Correlations between observed surface densities σ(H I) and $\sigma(H_2)$. The open circles and the triangles show our observations with the 45-m telescope in superclouds P and Q, respectively (paper I and the present paper). The crosses represent the observation in P by Boulanger et al. (1984) with the Onsala 20-m telescope.

and the velocity ranges of the observed CO emissions. This figure shows that most of the CO emissions seem to be associated with the -520-km s^{-1} component of H I. We note that the CO velocity, ~ -510 km s^{-1}, is slightly larger than that of H I. Recalling the direction of rotation in this region, we note that the CO velocity is delayed from that of H I.

Figure 8 gives the correlation between the surface density of H_2 and the total surface gas density of H I and H_2 in superclouds P and Q. A clear dependence of $\sigma(H_2)$ on the total gas density σ(H I+H_2) can be seen. The ratio of $\sigma(H_2)$ increases from 0.4 to 0.7 with the total gas density. The result of Boulanger et al. (1984) with a 100-pc resolution gives smaller ratios and shows no clear correlation, which may be due to a dilution of the CO intensity in the larger beam. Figure 8 can be interpreted in the following way. The face-on H I surface density is nearly constant ($\sim 10\ M_\odot$ pc^{-2}) within the supercloud as seen in figure 4. Therefore, figure 8 suggests that all the mass in excess of about $10\ M_\odot$ pc^{-2} is converted into molecular gas. This result and the narrow width of the CO arm give evidence of a changing state of gases in the superclouds.

The authors wish to express their hearty thanks to the staff of the Nobeyama Radio Observatory for the help in the observations. They thank Dr. E. Brinks for making the H I data available in the form of magnetic tapes. The data processing was carried out on a FACOM-M200 at NRO, and on a FACOM-M382 at the Data Processing Center of Kyoto University.

References

Baade, W., and Arp, H. 1964, *Astrophys. J.*, **139**, 1027.
Blitz, L. 1985, *Astrophys. J.*, **296**, 481.
Boulanger, F., Bystedt, J., Casoli, F., and Combes, F. 1984, *Astron. Astrophys.*, **140**, L5.

Boulanger, F., Stark, A. A., and Combes, F. 1981, *Astron. Astrophys.*, **93**, L1.
Brinks, E., and Burton, W. B. 1984, *Astron. Astrophys.*, **141**, 195.
Brinks, E., and Shane, W. W. 1984, *Astron. Astrophys. Suppl.*, **55**, 179.
Elmegreen, B. G., and Elmegreen, D. M. 1983, *Monthly Notices Roy. Astron. Soc.*, **203**, 31.
Habing, H. J., Miley, G., Young, E., Baud, B., Boggess, N., Clegg, P. E., de Jong, T., Harris, S., Raimond, E., Rowan-Robinson, M., and Soifer, B. T. 1984, *Astrophys. J. Letters*, **278**, L59.
Ichikawa, T., Nakano, M., and Tanaka, Y. D. 1987, in *Star Forming Regions, IAU Symp. No. 115*, ed. M. Peimbert and J. Jugaku (Reidel, Dordrecht), p. 622.
Ichikawa, T., Nakano, M., Tanaka, Y. D., Saitō, M., Nakai, N., Sofue, Y., and Kaifu, N. 1985, *Publ. Astron. Soc. Japan*, **37**, 439 (Paper I).
Pellet, A., Astier, N., Viale, A., Courtès, G., Maucherat, A., Monnet, G., and Simien, F. 1978, *Astron. Astrophys. Suppl.*, **31**, 439.
Stark, A. A. 1985, in *The Milky Way Galaxy, IAU Symp. No. 106*, ed. H. van Woerden, R. J. Allen, and W. B. Burton (Reidel, Dordrecht), p. 445.